ABSTRACT

AVASARALA, NAGA SRUTI. Electrical Conductivity of Graphene composites with Indium and Indium Gallium alloy. (Under the direction of Dr. Jagannadham Kasichainula.)

Composites of graphene with Indium and Indium Gallium alloy were synthesized for use in bonding chips and heat spreaders and their electrical conductivity was measured. The contribution of graphene was evaluated and its volume fraction and resistivity evaluated. Graphene has exceptionally high electron mobilities and higher electrical conductivity than silver.

Graphite was oxidized to graphene oxide using sulphuric and nitric acids. Graphene oxide was then suspended in propanol and exfoliated using ultrasonification. The solution was deposited on Indium and Indium Gallium films and folded and rolled. Graphene oxide was reduced by Indium flux at temperature just below the melting point and etched by HCl. The samples were characterized for distribution, size and volume fraction of graphene by transmission electron microscopy (TEM), scanning electron microscopy (SEM), optical microscopy and X-ray diffraction (XRD). Volume fractions were computed using linear intercept method from SEM and optical images.

Electrical conductivity of the samples was measured using four probe contact technique. The conductivity of the composite was modeled using rule of mixtures and effective mean field analysis. The resistance and temperature coefficient of resistance measured were used to evaluate the volume fraction and resistivity of graphene. Graphene is shown to increase the conductivity of the composite significantly and EMA analysis gives a better estimate of the resistivity of graphene.

Electrical Conductivity of Graphene Composites with Indium and Indium Gallium Alloy

by
Naga Sruti Avasarala

A thesis submitted to the Graduate Faculty of
North Carolina State University
in partial fulfillment of the
requirements for the Degree of
Master of Science

Materials Science and Engineering

Raleigh, North Carolina

2010

APPROVED BY:

Dr. Ronald O. Scattergood

Dr. Veena Misra

Dr. Jagannadham Kasichainula

Chair of Advisory Committee

BIOGRAPHY

Naga Sruti Avasarala was born in Hyderabad, Andhra Pradesh, India on April 3rd, 1988. She completed her schooling in Bharatiya Vidya Bhavans Public school in Hyderabad. She joined Indian Institute of Technology Madras, Chennai for her undergraduate education in Metallurgical and Materials Engineering. She graduated with a minor in chemistry in 2009. In the fall of 2009, she joined NCSU to pursue Master of Science degree in Materials Science and Engineering, while working toward a minor in Electrical Engineering.

ACKNOWLEDGEMENTS

I would first like to thank my advisor, Dr. Jag Kasichainula, for all of his guidance and support, which drove this research. I also want to thank Dr. Ron Scattergood and Dr. Veena Mishta for being committee members, as well as for their guidance. I thank Tom and Gunjan for assistance with characterization techniques. I also thank the Materials Science and Engineering department and Edna Deas for all of their help. Finally, I would like to thank my family and friends for their support throughout my graduate studies.

TABLE OF CONTENTS

LIST OF TABLES

LIST OF FIGURES

Chapter 1

Introduction

1.1 Graphene

Graphene is a one atom thick planar sheet of sp^2-bonded carbon atoms that are densely packed in a honeycomb crystal lattice[(1)] and is a basic building block for graphitic materials of all other dimensionalities. The carbon- carbon bond length in graphene is 0.142 nm, similar to that in graphite. Graphene is an isolated atomic plane of graphite with close packed hexagonal arrangement.

1.2 Methods of Preparation

One atom-thick materials such as graphene have remained unknown because nature strictly forbids the growth of low dimensional crystals. Crystal growth implies high temperature and therefore thermal fluctuations are detrimental for the stability of graphene. As the lateral size increases, the phonon density integrated over the 3D space available for thermal vibrations rapidly grows, diverging on a macroscopic scale. This forces two-dimensional (2D) crystallites to morph into a variety of three-dimensional (3D) structures.

Taking this into consideration, there are two principal routes for making 2D crystals. One is to mechanically split strong layered materials such as graphite into individual atomic planes. This is how graphene was first isolated and studied[(2)]. Although delicate and time-consuming, this method provides crystals of high structural and electronic quality. Instead of cleaving graphite mechanically, it is also possible to automate the process by using ultrasonic cleavage. Ultrasonification in water leads to stable suspensions of sub micrometer graphene. The ultrasonic cleavage of chemically “loosened” graphite, in which atomic planes are partially detached first by intercalation makes the sonification more efficient. Exfoliation of graphite is an alternative route to the separation of graphene layers[3]. However, the lack of functional groups in the graphene sheets promote the reaggregation of the material into micron sized clusters. Different methods have been used for the exfoliation of graphite. One method was overnight treatment at room temperature with a mixture of concentrated sulphuric acid and nitric acid (3:1)[3]. The intercalated graphite was then exfoliated by thermal shock on rapid exposure to high temperatures in nitrogen. The exfoliated graphite was dispersed in acetone by high shear mixing followed by bath sonication. Another method is to prepare Graphite oxide using Hummers method[4]. Graphite oxide prepared this way was mixed with water and sonicated. Hydrazine hydrate was then added and the solution heated in a oil bath at 100^{o}C till the reduced graphite oxide was precipitated out as a black solid. This was isolated by filtration[5].

A sheet of graphene oxide consists of a hexagonal ring based carbon network having both sp^2-hybridised carbon atoms and sp^3-hybridised carbon atoms bearing hydroxyl and epoxide functional groups on either side of the sheet, whereas the sheet edges are mostly decorated by carboxyl and carbonyl groups[6]. Graphite oxide is hydrophilic in nature due to the oxygenated graphene layers and water molecules can readily intercalate into the interlayer galleries. Hence it forms stable colloidal suspensions of thin sheets in water. Ultrasonic treatment leads to formation of stable dispersions.

An alternate route is to start with graphene layers grown on top of other crystals. After the epitaxial structure is cooled down, one can remove the substrate by chemical etching. Epitaxial graphene layers grown on SiC[1] have been considered a champion route to graphene wafers for electronic applications, mostly because SiC with close packed hexagonal structure automatically provides an insulating substrate.

1.3 Physical Properties of Graphene

Graphene is the thinnest known material in the universe and the strongest ever measured [(2)]. Its charge carriers exhibit giant intrinsic mobility, have zero effective mass, and can travel for micrometers without scattering at room temperature[(2)]. Graphene can sustain current densities six orders of magnitude higher than that of copper, shows record thermal conductivity and stiffness, is impermeable to gases, and reconciles such conflicting qualities as brittleness and ductility[(2)]. The most explored aspect of graphene physics is its electronic properties. The corresponding resistivity of graphene sheet would be less than 10^{-6} Ω cm[(7-9)], less than the resistivity of silver, the lowest resistivity substance known at room temperature. Several features make graphene's electronic properties unique and different from those of any other known condensed matter system.

The first is graphene's electronic spectrum. Intrinsic graphene is a semi-metal or zero gap semiconductor with its conduction and valence bands meeting at the Dirac point[(8)]. This characteristic enables the electron transport to be tuned between hole or electron conduction by shifting the Fermi level by an applied electric field.

Graphene's unusual electronic properties arise from the fact that the carbon atom has four electrons, three of which are tied up in bonding with its neighbors. But the unbound fourth electrons are in orbitals extending vertically above and below the plane, and the hybridization of these spreads across the whole graphene sheet. The hybridized electrons interact with the periodic field of the hexagonal crystal lattice and form Dirac fermions, described by cone-like energy bands[(10)]. These electrons are described by Dirac-like equation rather than Schrodinger equation that describe the wave mechanics of the fundamental particles. Hence, the electrons and holes are called Dirac fermions, which at low energies are accurately described by the (2+1)-dimensional Dirac equation with an effective speed of light vF ≈ 106 $m^{-1}s^{-1}$. They can be seen as electrons that have lost their rest mass m_o or as neutrinos that acquired the electron charge, e[(8)].

However, the observed low mobility of charge carriers in graphene is associated with impurity scattering [8]. Graphene has remarkably high electron mobility at room temperature with reported values in excess of 15,000 $cm^2V^{-1}s^{-1}$ [9,10] which would lead to enhanced electrical conductivity. The mobility is nearly independent of temperature between 10 K and 100 K, which implies that the dominant scattering mechanism is defect scattering. Other scattering centers such as edges, hepta and penta rings, ripples and surface corrugations[12,13] that are expected in free standing two-dimensional films are also important.

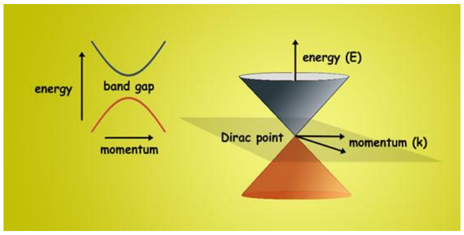

Fig 1.3(i): Band Structure of Graphene (Reference: 9)

The energy-wave number (E-k) relation is linear for low energies near the six corners of the Brillouin zone, leading to zero effective mass for electrons and holes[11].

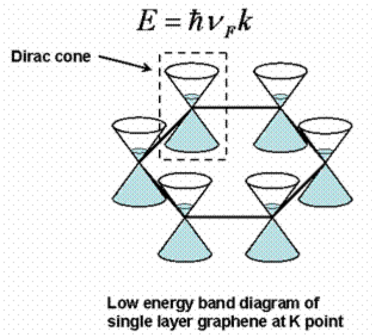

Fig 1.3(ii): Band Diagram of Graphene near the corners of Brillouin zone (Reference: 10)

In addition, the finite size of the graphene film samples and chemical doping also lead to a band gap. The mobility of graphene, μ at 300 K is still limited by impurity scattering, and therefore can be improved significantly, perhaps, even up to ≈100,000 $cm^2V^{-1}s^{-1}$. Although some semiconductors exhibit room temperature μ as high as ≈77,000 $cm^2V^{-1}s^{-1}$ (namely, InSb), those values are quoted for undoped bulk semiconductors. In graphene, μ remains high even at high n (>10^{12} cm^{-2}) in both electrically and chemically doped devices, which translates into ballistic transport on the submicrometer scale (currently up to ≈0.3 μm at 300 K).

Secondly, graphene exhibits an astonishing electronic quality. Its electrons can cover submicrometer distances without scattering. As a result of the massless carriers and little scattering, quantum effects in graphene are robust and can survive even at room temperatures. The electronic structure rapidly evolves with the number of layers, approaching the 3D limit of graphite at about 10 layers. Only graphene and its bilayer have simple electronic spectra. They are both zero-gap semiconductors with one type electron and one type of hole. For three or more layers, the spectrum becomes increasingly complicated. Several charge carriers appear and the conduction and valence bands start notable overlapping(1).

The near-room temperature thermal conductivity of graphene was recently measured to be between $(4.84\pm0.44)\times10^3$ and $(5.30\pm0.48)\times10^3$ $Wm^{-1}K^{-1}$(14,15).This is in excess of those measured for carbon nanotubes or diamond(9). The thermal conduction is phonon-dominated near room temperature and above. Graphite, a 3D version of graphene, has basal plane thermal conductivity of over a 1000 W/mK. In graphite, the c-axis thermal conductivity is over a factor of 100 smaller due to weak binding forces between the basal planes as well as the larger lattice spacing.

Graphene appears to be one of the strongest materials ever tested. Graphene has a breaking strength 200 times greater than steel. Its spring constant was in the range 1-5 N/m and the

Young's modulus was 0.5 TPa[16,17], which differs from that of the bulk graphite. These high values make graphene very strong and rigid.

1.4 Applications of Graphene

Due to its remarkable properties described above, graphene has many potential applications. However they are still in the development stage.

Graphene makes an excellent sensor due its 2D structure. The fact that the entire volume is exposed to its surroundings makes it very efficient to detect adsorbed molecules. Due to its high electronic quality, graphene has also attracted the interest of technologists who see them as a way of constructing ballistic transistors. Graphene has a high carrier mobility, as well as low noise, allowing it to be used as the channel in a field effect transistor (FET). Graphene films are currently explored for metallization lines in devices[18], high speed devices associated high mobility of the carriers, and several other applications including spintronics[19] and sensors[20]. In contrast to carbon nanotubes that show poor interfacial interaction with the matrix and curving around in different types of composites, graphene may provide large surface area of interaction with other atoms.

Graphene is an ideal material for spintronics due to small spin-orbit interaction and near absence of nuclear magnetic moments in carbon. Electrical spin-current injection and detection in graphene was recently demonstrated up to room temperature.

The most immediate application would be incorporation of graphene in composite since it is easier to produce than free standing graphene. Graphene composites have a wide variety of applications. Electrical conductivity of composites of graphite with metals such as Cu has been studied for application in electrofriction materials[5,21]. High electrical conductivity, thermal conductivity, and low coefficient of friction are the desired properties.

1.5 Indium-Graphene Composite

Low melting point solders that flow easily are important for thermal interface materials in bonding devices to a heat spreader. In (mp 159^{o}C) and In-Ga alloys have very low melting characteristics (mp<159^{o}C) and possess the ability to deform and accommodate thermal strains that arise during cooling subsequent to bonding of the devices to heat spreaders. However, the progress in miniaturizing device components has aggravated the problems associated with heat dissipation in the electronics industry, and this has produced a need for improved thermal interface materials in modern chip packaging. Hence, increasing the conductivity of In and In-Ga composites would increase the efficiency of these materials for the growing demand. Hence graphene was added to form a composite of superior properties.

Although graphene possesses many novel properties of interest, the presence of surface interactions with matrix atoms in a composite could be responsible for degradation similar to that observed in graphite which is a three-dimensional arrangement of graphene planes[7,22,23]. In addition, the finite size and thickness of the graphene platelets and dispersions in a matrix will also limit the properties of the composite. We are interested in understanding the electrical conducting property of graphene in the composites with metals and determine its contribution using effective mean field analysis. Towards this goal, we have synthesized composites of graphene with In and In-Ga alloys and studied the electrical conductivity of the composites.

1.6 Graphene Metal Contacts

A difference in the work functions of the metal and graphene leads to charge transfer at the contact interface. Metal-graphene contacts can be divided into two groups, the weak contact and the strong contact[22]. The characteristic electronic structure of graphene is significantly altered by chemisorption on Ti, Co, Ni and Pd but is preserved by weak adsorption on Al, Cu, Ag and Pt. The metals which form a weak contact cause the Fermi level to move away from the Dirac point in graphene without changing the band structure, resulting in doping with either electrons or holes.

While in strong chemisorptions, electronic structure of graphene is significantly altered, even Dirac point cannot be found in the band structure[23] .The DOS(Density of states) peak of Ti's 3d orbital is located around the Fermi level, where graphene's p_z orbital also peaks. Strong chemical bond could form between d-orbital and p_z orbital. Sc, Co and Ni also show this kind of interaction because their 3d orbital have a similar energy as Ti. In contrast, Au's 4d orbital peak sits far away from the Fermi level to make the interaction unlikely to happen.

Since Indium belongs to the same group as Al, graphene would be weakly adsorbed on its surface. The measurements of contact resistance of metals on graphene have been done in literature. The I_d-V_d characteristics of Ni on graphene were studied and the linearity of the curves indicated the formation of an ohmic contact[24]. Hence Indium-graphene contact can be expected to behave as an ohmic contact.

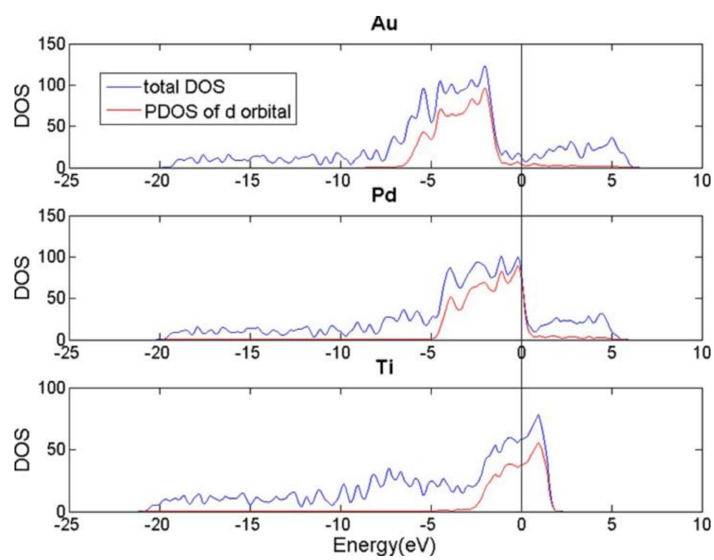

Reference: 22

Fig 1.6(i): The DOS of (a) Au/graphene contact (b) Pd/graphene contact, and (c) Ti/graphene contact (the vertical line indicates the Fermi level).

Chapter 2

EXPERIMENTAL PROCEDURE

2.1. Preparation of Indium-Graphene composite

Several methods to prepare graphene have been proposed in literature. However bulk production has been the main problem. Chemical exfoliation of graphite through oxidation and then dispersion to single graphene is the method used in the present work.

Composites of In-graphene were processed using graphene prepared by the chemical exfoliation of graphene oxide. Microcrystalline graphite, supplied by Asbury Graphite Inc was oxidized by reacting with a boiling mixture of concentrated sulphuric acid and nitric acid in equal proportions for 4 hours. Oxidation was completed when the color of graphite turned brown. The mixture was cleaned with distilled water and filtered several times to remove the acids. The graphite oxide residue was mixed with distilled water and ultrasonicated till the suspension did not sediment and did not settle for several days. The suspension was filtered and dried for several hours at $150^{o}C$. The graphite oxide was mixed with propanol and sonicated for several hours to form a suspension again. This suspension of exfoliated graphene oxide[6,25] is further added to the samples of indium foil.

Indium foil 99.99 % purity and 0.25 mm thickness was supplied by Alfa Aesar. Samples of dimensions 1.5 cm × 1.5 cm were cut from this foil. These foils were placed between polyethylene sheets and rolled to thickness of 0.1 mm. The polyethylene sheets were used to avoid indium, which is a soft metal from sticking to the rollers. The indium foil was then bent in the shape of a boat by tweezers to prevent the suspension from slipping. A glass tube of 2 mm diameter was inserted into the graphene oxide suspension and a part of it was retained and deposited in to the boat of In foil. The graphene oxide was deposited repeatedly to generate enough volume fraction of graphene in the composite when propanol evaporated The deposition of graphene was continued over 20 times. The In boat with graphene oxide was folded several times and rolled further into thin foils. The foils were annealed at 100^{o}C so they could re-crystallise and be rolled further.

The reduction of graphene oxide to graphene by oxidation of indium is thermodynamically favorable[(26)] and the removal of indium oxide using indium flux is also thermodynamically favorable. The free energy of formation of Indium Oxide(In_2O_3) at room temperature (298 K) is found to be -221.5 kcal/mol and of Gallium Oxide(Ga_2O_3) is -258.8 kcal/mol[(26)]. Hence the oxide formation of In and Ga when reacted with graphene oxide would be spontaneous. Small quantity of indium flux was placed in the folded In foil with graphene oxide and heated to slightly above the melting point, 159^{o}C so that the indium oxide formed by reduction of graphene oxide was fluxed and graphene was left in the Indium foil. The fluxed Indium oxide was etched away by dilute HCl from the surface.

2.2. Preparation of In-Ga-Graphene Composite

In-Ga alloy samples were first prepared by mixing Ga in liquid form to In foil, thus, reducing the melting point of the system further. The Ga liquid was added in small amounts to the boat shaped In foil. The In foil with Ga was repeatedly folded, hot rolled and weighed. The Ga liquid was added till a composition of 3.1 wt % Ga was reached. The 3.1 wt% Ga corresponds to 5 at% Ga which is less than the solubility limit of Ga in Indium. The solubility limit is near 15 at% at the eutectic temperature (290 K). Ga along the grain boundaries in indium causes brittle behavior and leads to cracking of the alloy at room temperature due to lack of sufficient ductility. Hence the rolling was carried out at 80^{o}C. Rolling with a small steel roller was carried out on a hot plate with the foils placed between two glass slides.

Graphene was added to In-Ga foils following the same procedure as described above for

Indium foils. In flux was used to remove oxide films of In or Ga and HCl was used to etch away the fluxed oxide on the surface.

The thickness of the In-graphene foils was close to 0.15 mm while that of In-Ga-graphene foils was close to 0.30 mm. Three samples of In-graphene and five samples of In-Ga-graphene were finally annealed at 80^{o}C.

2.3. Electrical Resistivity Measurements

Resistance measurements were carried out with a system comprising a Keithley 2400-LV Source Meter, a Keithley 2182-Nanovoltmeter, a K-20 Temperature Control System and a low temperature chamber both from MMR Technologies Inc., and HT Basic software. The source meter was used to apply a current of 10 mA and increased in steps of 10 mA up to 50 mA, while the nanovoltmeter was used to monitor the voltage in the system. The given current with the measured voltage was used to generate the resistance measurements using Ohm's Law,$V = I\ R$ where V is the voltage, I is the current and R is the resistance.

A Signatone four probe pin contact instrument was used to make measurements of resistivity at room temperature (300 K). The outer probes were used to input the current from the source meter while the inner probes were used to measure voltage across using the nanovoltmeter. The separation between the inner probes was 1.66 mm and diameter of the pins was 0.085 mm. The reverse current method was used to cancel the thermal electromotive force (EMF) at the contacts by sending current in the forward and reverse directions. The average value of voltage measurements for both cases is taken to measure the resistance and resistivity.

The area of cross-section of the samples was determined from the width and thickness of the sample. Resistivity was obtained from R=ρl/a where ρ is the resistivity, l is the separation between the probes and a is the area of cross-section. Samples of approximately 1 mm width were sliced from the larger composite foils. The thickness and width of the samples was measured using a micron marker in the optical microscope. The smaller width increased the magnitude of measured resistance of the samples and hence improved the sensitivity of measurements. The graphene particle size and separation were much smaller and hence smaller width would lead to better evaluation of contribution of graphene to resistivity.

Temperature coefficient of resistance of the samples was measured using the collinear four probe method in a temperature controlled chamber described below.

The sample for performing these tests was with dimensions of 1 cm x 2 cm rectangle. Four small dots of colloidal silver paste were applied along the diagonal of the rectangle, and 0.025 mm diameter gold wires, about 2 cm long were attached to the silver dots. Once the silver paste was completely dried and the gold wires were secured, zinc oxide (ZnO) paste was applied to the substrate holder in the chamber with a silicon heat sink immediately above. The sample was placed on the Si heat sink on the holder. The purpose for applying the ZnO was because it is electrically insulating and thermally conductive, thus, preventing false readings of electrical resistance, while allowing equilibration of temperature from the dewar to the sample. Next, the free ends of the gold wires were connected to the leads on the Kapton printed circuit board of the low temperature dewar using indium solder, which alloys well with gold. Finally, the dewar was closed, the proper connections to the inner leads for electrical measurements and the vacuum were made, and the test was performed. Fig 2.3(i) provides a visual representation of the inside of the dewar.

The resistance test performed on the samples was sheet resistance, in which four probes were used rather than two probes to avoid false measurements from contact resistance that occurs with two probe measurements. The reverse current approach was again used to cancel the thermal EMF from the probe contacts.

The temperature coefficient of resistance was measured by performing the voltage measurements at different temperatures obtained by the K-20 temperature controller. The K-

20 Temperature Control System enabled the runs to range between room temperature and 340 K and a lower temperature at 260 K, while capturing resistance measurements at intervals of 10 K. The test operated under 6 mTorr vacuum, and the dewar was cooled by adiabatic expansion of nitrogen gas flow through a nozzle that remained near 3.4 sccm, under a pressure of 1800 psi. The results from these tests are in the form of graphs of resistance as a function of temperature. The temperature coefficient of resistance was obtained from the slope of the graph with resistance as a function of temperature.

Fig 2.3(i) : Picture of the inside of the dewar

2.4. X-Ray Diffraction

X-ray diffraction of the composite samples was carried out using Cu K_{α} (λ=0.154 nm) radiation in a Rigaku instrument with operating current of 25mA and a voltage of 25 kV. Debye-Scherrer θ-2θ diffraction scans were carried out at intervals of $2\theta= 0.1^0$. The sample was held on Si (001) wafer using mounting clay.

2.5 Microscopy

Optical, scanning and transmission electron microscopy was carried out to determine the size, distribution and volume fraction of graphene platelets in the composite.

Optical micrographs were obtained by placing the samples in the viewing area of a CARL ZEISS optical microscope with DIC (differential interface contrast), model 60523. Optical micrographs of several regions on each sample were captured using a digital camera.

The samples were also placed in the Hitachi S-3200N SEM chamber at Analytical Instrumentation Facility and examined in secondary electron mode, which is more sensitive to topography, as well as in backscattered mode, which is more sensitive to atomic number. In secondary electron mode, samples were imaged at different magnifications. In backscattered mode, EDS (energy dispersive spectrometry) spectrums were taken on the various samples.

The graphene oxide which was suspended in propanol was collected on a carbon-holly grid and observed under the transmission electron microscope. Suspension of the graphene oxide film in propanol was collected inserting a glass tube and the suspension was slowly released onto a carbon holly grid. The liquid was then allowed to dry leaving graphene oxide particulates on the grid. The graphene oxide films were extremely thin and further sample preparation was not required to make them electron beam transparent. The grid was placed on a double tilt specimen holder and observed under a JEOL 2000FX transmission electron microscope.

Chapter 3

RESULTS

3.1 Resistance Measurements

The measurements were carried out on three samples each from the In and In-Ga foil. The samples are listed as In and Ga. The three In-graphene samples are named In-Gr-1. In-Gr-2 and In-Gr-3. The five In-Ga-graphene samples are listed as In-Ga-Gr-1, In-Ga-Gr-2 and so on. The resistance was measured as temperature was varied both during the heating and the cooling process. The calculated values of resistance for In-Gr-3 with the current and voltage values are given in Table 3.1(i) below.

Table 3.1(i): Resistance measurement of In-Gr-3 sample

T(K)	I (mamps)	V_1(mv)	V_2(mv)	V_{av}(mV)	R(Ω)
330	50	.05042	-.0307	.0405	.000811
320	50	.04406	-.0337	.0389	.00778
310	50	.04603	-.0288	.0374	.000749
300	50	.03923	-.0392	.036	.000721
290	50	.04057	-.0285	.0345	.000691
280	50	.03927	-.0271	.0332	.000664
270	50	.0362	-.0271	.0316	.000634

The values of resistance are plotted as a function of temperature and the slope was determined. The plots for 2 of the samples, In-Gr-3 and In-Ga-Gr-3 are shown below in Fig 3.1(i) and Fig 3.1(ii). Values of resistance during heating are shown in blue and during cooling in red. The values remained close to each other.

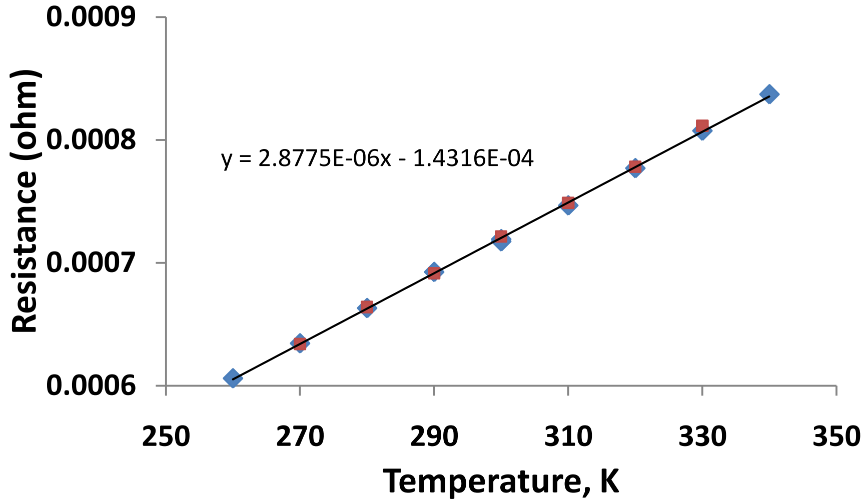

Fig 3.1(i): Variation of resistance with temperature of In-Gr-3 sample

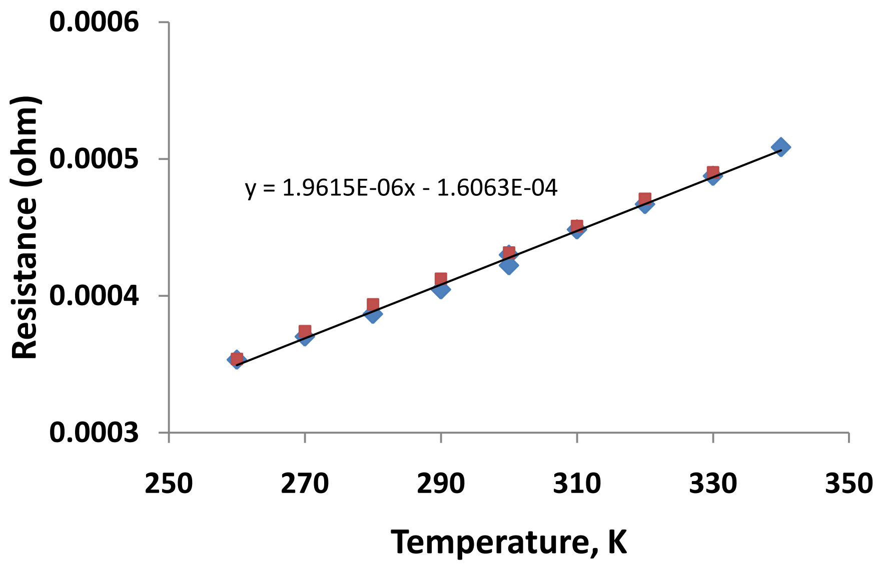

Fig 3.1(ii): Variation of resistance with temperature of In-Ga-Gr-3 sample

The temperature coefficient of resistance (TCR) is defined as

$$TCR = \frac{1}{R}\frac{dR}{dT}$$

The slope of the resistance vs. temperature plot is used to determine the TCR at room temperature (300 K) for all the samples. The measured values of resistivity and the temperature coefficient of resistance are presented below in Table 3.1(ii).

Table 3.1(ii): Variation of resistance with temperature

Sample Name	Sample Thickness(mm)	Sample Width(mm)	Resistivity (10^{-6} ohm cm)	TCR (10^{-3} K^{-1})
In	.26	1.3	9.42	4.35
In	.26	1.3	9.42	4.35
In	.26	1.3	9.42	4.35
In-Ga	.37	1.7	10.74	4.32
In-Ga	.37	2.7	10.74	4.32
In-Ga	.37	1.7	10.74	4.32
In-Gr-1	.15	.72	7.35	4.12
In-Gr-2	.14	.83	8.85	4.26
In-Gr-3	.13	.75	8.65	4.00
In-Ga-Gr-1	.30	.90	9.55	4.21
In-Ga-Gr-2	.29	.90	9.25	4.15
In-Ga-Gr-3	.36	.70	9.32	4.26
In-Ga-Gr-4	.32	1.05	9.53	4.15
In-Ga-Gr-5	.40	.85	9.81	4.24

The three different samples obtained from In and In-Ga showed same resistance values within the limit of approximation used.

3.2 X-Ray Diffraction

The X-ray peak profile is shown in the Fig 3.2(i) below.

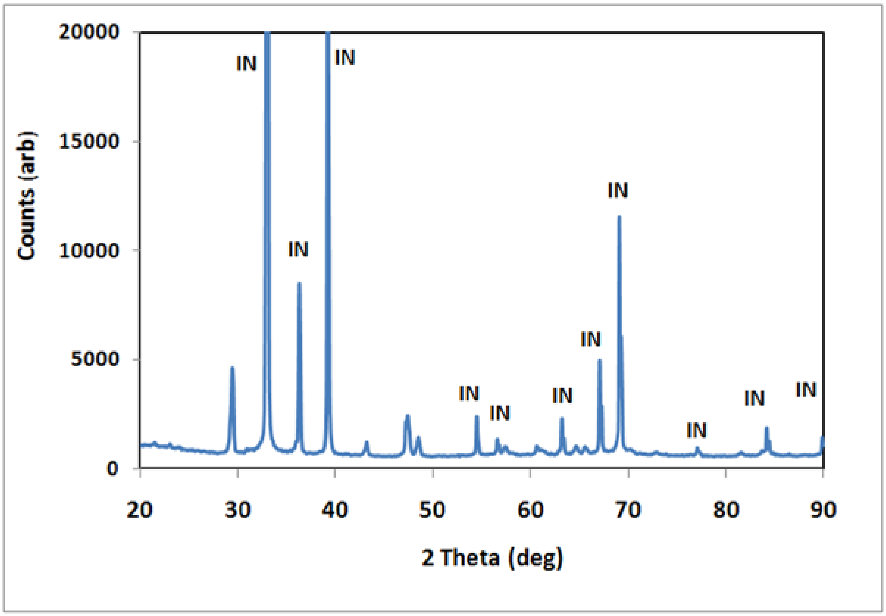

Fig 3.2(i): X ray diffraction peak profile of In-Gr-1 sample

All the major peaks correspond to In and are labeled "IN". All other peaks arise from the mounting clay. There are no graphite peaks observed in the profile. This could be because of the very thin graphene platelets and their discontinuous distribution in the In foil. The extremely small number of atomic layers contributing to X-ray diffraction (XRD) would not give enough counts to be recognized by the detector. There was a small increase in the amorphous background near $2\theta=20^o$. This could refer to the presence of an amorphous phase. Hence the amorphous region in the XRD profile could be attributed to presence of some oxide which was not reduced.

3.3 Microscopy

Secondary electron microscopy images of In film with suspended graphene oxide before subjecting to rolling are shown in Fig 3.3(i) and (ii) below. Since these images were taken before rolling and folding, it is assumed that reduction of graphene oxide has not yet taken place.

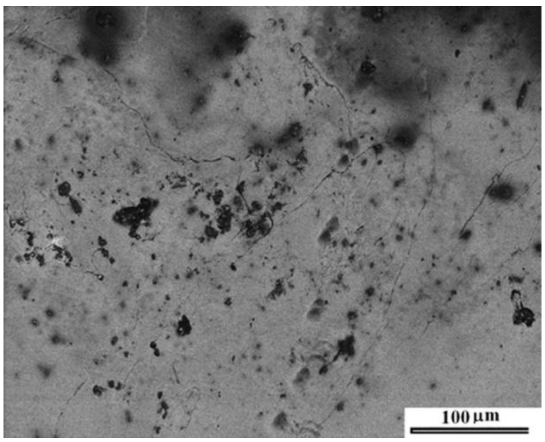

Fig 3.3(i) SEM image of graphene oxide on In film before rolling and folding

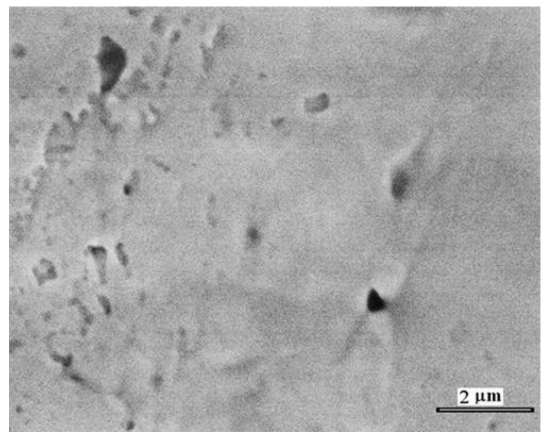

Fig 3.3(ii): Higher magnification image

Fig 3.3(i) shows a random distribution of graphene oxide particulates of different sizes. Some graphene oxide particulates showed dark contrast while others were lighter. Their sizes varied from 50nm to 3µm. However their thickness cannot be determined from these images. Secondary electron images (SEM) also have contribution from the backscattered electrons (BSE). Since carbon is a lighter element than indium, it appears darker in images where backscattered electrons contribute. The finite interaction volume implies contrast can also be present from graphene underneath the surface. Since the surface appears relatively flat and there is not much topographic contrast, there is very little secondary electron contrast. The dark contrast indicates a lower average atomic number or more carbon layers. Hence the darker regions indicate thicker graphene oxide with more number of layers. The higher magnification image shows the thinner platelets in more detail. The graphene platelets are mostly widespread and not connected. Their morphology is irregular. Cracks are visible on the In foil surface which could have formed during the rolling process.

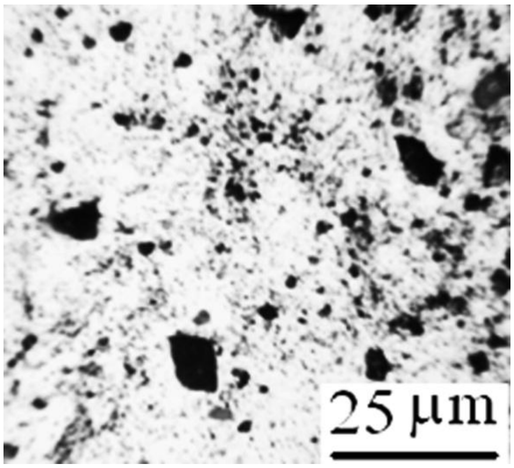

Fig 3.3(iii): Optical image of In-Gr-3 foil

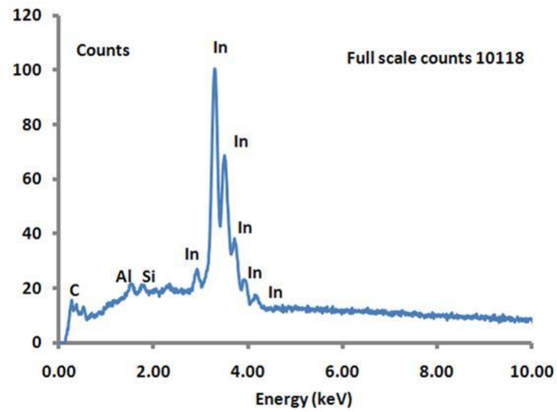

Fig 3.3(iv): EDS spectrum of In-Gr-3 foil

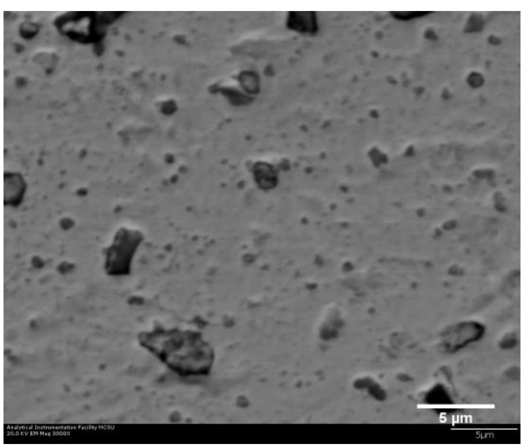

Fig 3.3(v): BSE of In-Gr-3

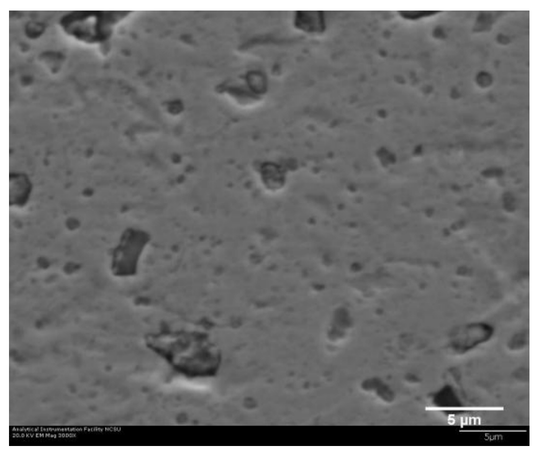

Fig 3.3(vi): SE of In-Gr-3

The optical image in Fig 3.3(iii) shows only the surface detail. The darker regions are thicker graphene platelets while the lighter regions are thinner graphene platelets. Volume fraction of graphene was calculated from the techniques of quantitative metallography. In particular, several lines were drawn at different angles and positions on the image. The ratio of the intercept of the line on the graphene particulates to the total length of the line was used to measure the volume fraction of graphene. The values are given in Table 3.3(i). The size of graphene particulates varied from submicron to 5μm. These sizes are similar to the graphene oxide platelets shown in Fig 3.3(i) and (ii).

However the distribution of graphene platelets is much more uniform than the graphene oxide platelets. Hence the rolling process results in the uniform distribution of graphene particulates without change in the size of the platelets. Since the rolling was done along several directions, this could have led to a more uniform distribution of the particulates. The backscattered and secondary electron images show similar contrast in the image since it is largely atomic number based. The edges appear darker which could be due to the folding of the 2-dimensional sheet. While the thicker particulates looked connected in the optical image, they are isolated and have a homogeneous distribution in the higher magnification SEM images. The volume fraction of graphene was calculated using linear intercept method as mentioned before. However it would not be very accurate using SEM images since the image is from a finite volume of interaction in the sample. Graphene from underneath the surface also contributes to the contrast of the images and hence does not give accurate volume fraction information.

Energy Dispersive X-ray spectroscopy (EDS) was carried out to determine the presence of impurities. The EDS spectrum is shown in Fig 3.3(iv). The counts are shown raised to the power of half. The peaks identified are In, Al, Si and C. The Al and Si peaks arise from the sample holder while the carbon peak in the beginning of the spectrum could be due to residual carbon on the surface. The most significant peaks with maximum counts were from Indium.

The optical, backscattered and secondary electron images of In-Ga-Gr-3 are shown below in Fig 3.3(vii), (viii) and (ix). The contrast from the images shows a much denser distribution of graphene than in In-Gr-3 sample. The graphene platelets appear connected in the optical image. However, they are isolated in the higher magnification SEM image. The isolated particulates are close together which could lead to the appearance of connectivity in the optical images. There are areas of thick and thin graphene platelets as seen in other images. The predominant feature though seems to be the thinner graphene platelets. The distribution of graphene is very uniform and the graphene platelets appear to be longer as opposed to irregular shaped (mostly elliptical) individual particulates in In-Gr-3 sample.

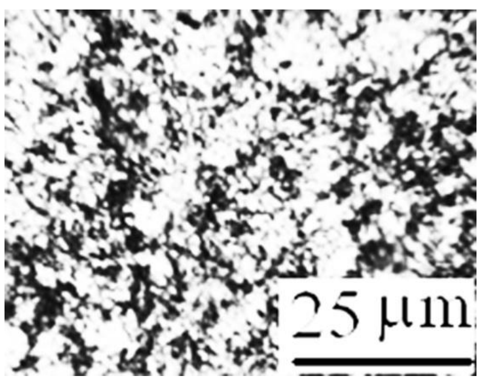

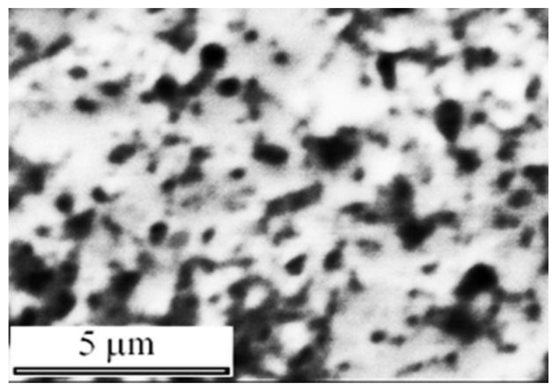

Fig 3.3(vii): Optical Image of In-Ga-Gr-3 Fig 3.3(viii): SEM image of In-Ga-Gr-3

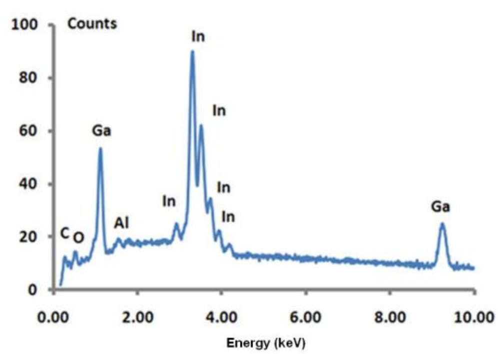

Fig 3.3(ix): EDS spectrum of In-Ga-Gr-3

The EDS spectrum for In-Ga-Gr-3 is shown in Fig 3.3(ix). The counts are shown raised to the power of half. The Al peak in the spectrum is from the specimen holder. The O peak is from oxide left on the surface which was not etched away. The peaks with high counts are from Indium and Gallium.

The exact mass of graphene in these samples could not be determined directly as the mass of graphene is too low to be detected. The volume fractions determined from optical and SEM images are given in the Table 3.3(i) below.

Table 3.3(i): Volume fractions determined from intercept method

Sample	Optical Image	SEM Image
In-Gr-1	.258	.183
In-Gr-2	.278	.236
In-Gr-3	.214	.172
In-Ga-Gr-1	.258	.2
In-Ga-Gr-2	.268	.208
In-Ga-Gr-3	.242	.236
In-Ga-Gr-4	.223	.299
In-Ga-Gr-5	.279	.219

The volume fractions obtained from both the methods of imaging (optical and SEM) are found to differ. This is due the differences observed in the distribution of graphene in the images. The lower magnification optical images give a better idea of the sample since they cover a larger volume of the sample but they do not show in detail the distribution of thinner graphene platelets whereas the higher magnification SEM images are constrained to a small volume of the sample but show thin graphene platelets. The measurements are expected to be valid only to an accuracy of 0.05. Modeling was further used to calculate the volume fractions so that these results could be verified.

The distribution of graphene particulates obtained from In-Gr-3 sample is presented in the figure 3.3(x). The distribution shows that a single maximum in the number fraction of particulates is present near 0.5 μm. Also majority of the particles are below 1 μm in size.

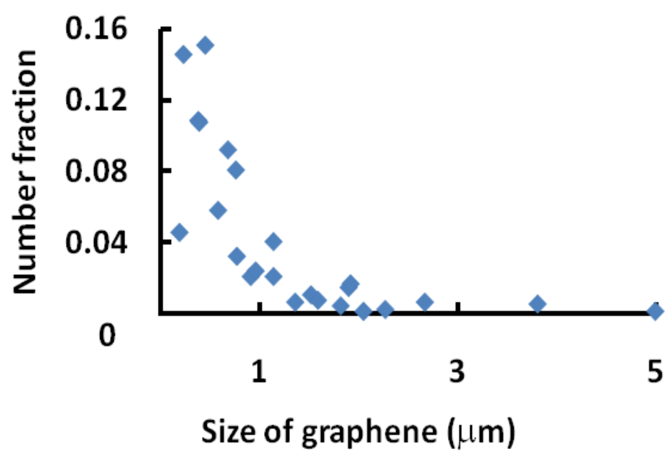

Figure 3.3(x). Number fraction of graphene particulates in In-Gr-3 samples observed in SEM images shown as a function of the size of the particulates.

Transmission electron microscope images of the sample were taken to determine the thickness and diffraction patterns of the sample. Since the sample is graphene oxide, care was taken not to contaminate it by moving the beam around and not going to a very high magnification. A low magnification image shown in Fig 3.3(xi) was taken at 1000X. The TEM image shows a majority of very thin films and a few thicker films.

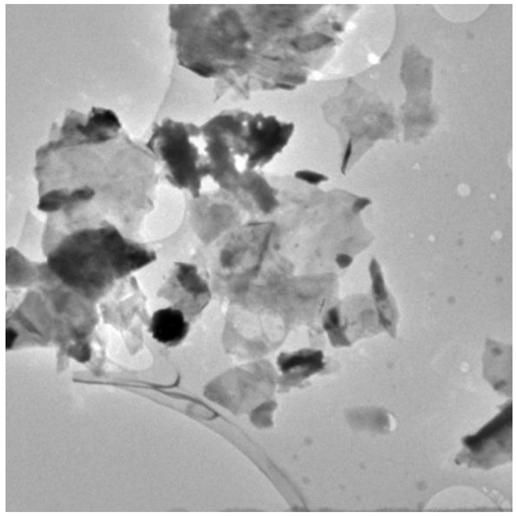

Fig 3.3(xi): TEM image of graphene

Diffraction patterns were obtained at the thick and the thin parts of the sample. The selected area electron diffraction (SAED) patterns were obtained at a camera length of 25 cm. The diffraction pattern showed the hexagonal pattern of graphite and is indexed in Fig 3.3(xii) below. The spot pattern was taken from a very thin portion of the sample.

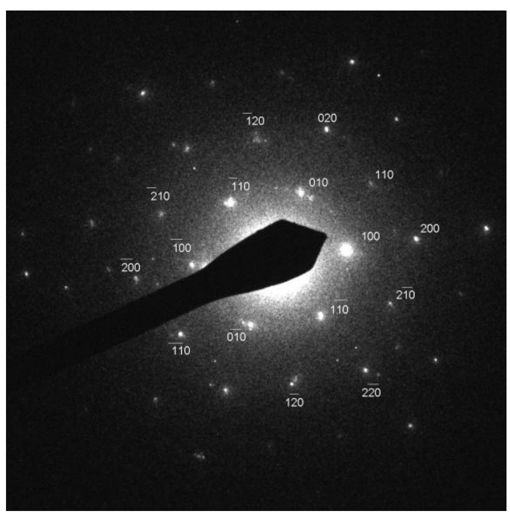

Fig 3.3(xii): Indexed SAED pattern of graphene

The diffraction patterns taken from thicker parts of the sample which may have multiple layers are shown below. Fig 3.3(xiii) shows the onset of ring pattern which could be due to the presence of larger number of particulates at different orientations. The presence of pairs of closely spaced spots could be because of the different orientations of the graphene oxide foils with each other. The effects of dynamical diffraction can be seen in the form of satellite spots around the main spots. The dynamical diffraction effect is visible in this pattern because of the increased thickness of the sample due to greater number of foils. The onset of the ring pattern is clearer in Fig 3.3(xiv). Though there are a few distinct spots visible in the lower order zone, the outer rings show less distinct spots.

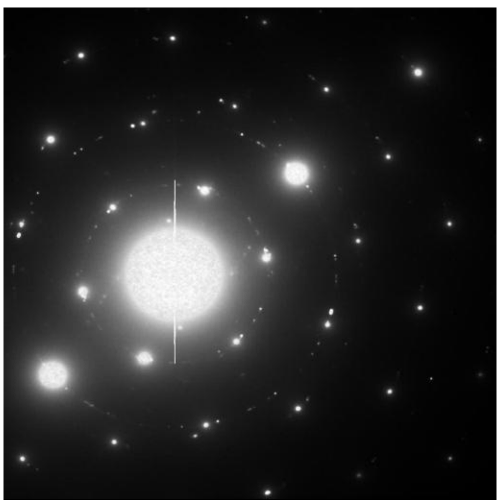

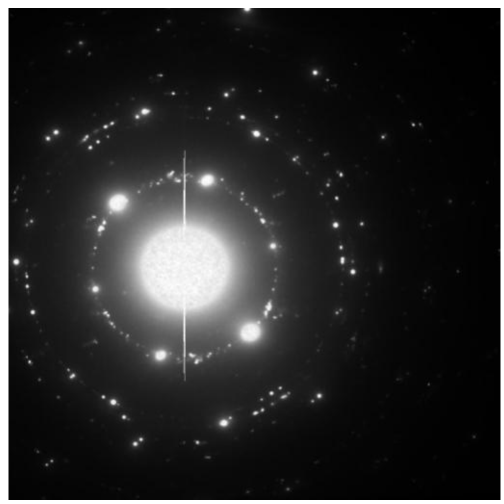

Fig 3.3(xiii) and (xiv): SAED patterns from thicker portion of samples

The bright field and dark field images were taken and are seen in the images below.

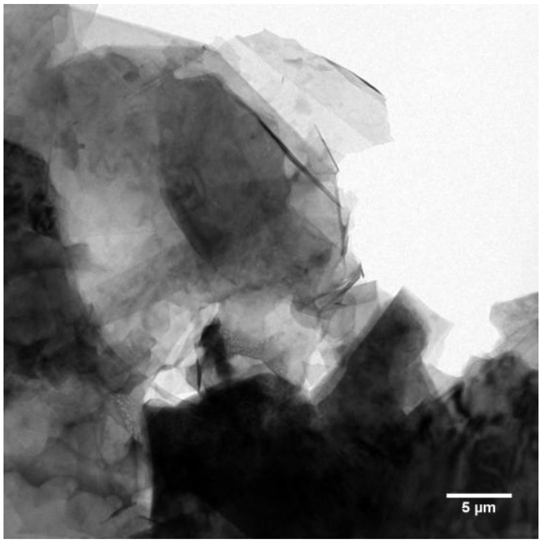

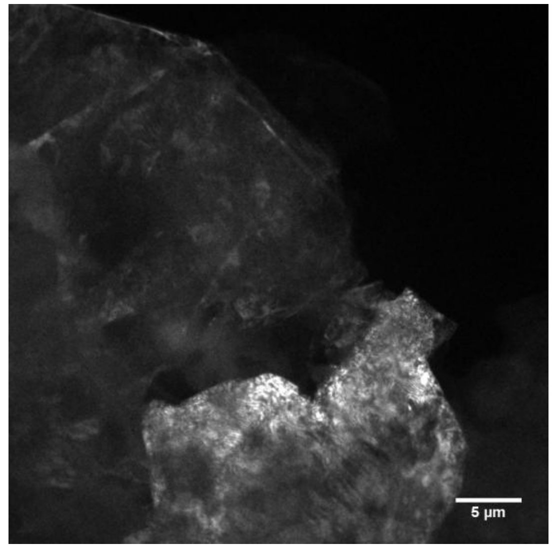

Fig 3.3(xv): Bright Field Image

Fig 3.3(xvi): Dark Field Image

The contrast in the images between the bright field and the dark field is clearly visible. The thinner single foil appears lighter in the bright field and darker in the dark field image. The bright field image shows better contrast than the dark field image. The major source of contrast is mass thickness contrast. Since the foils are at different orientations there could be diffraction contrast.

The thinnest part of the sample is at the edge which is visible in the bright field image. However it does not exhibit noticeable contrast in the dark field image. Hence it is too thin to scatter electrons. The folding up of the graphene oxide sheets at the edges can be observed though to a small extent.

A higher magnification image at 30kX was taken and is shown above in the Fig 3.3(xvii).
This image clearly shows the contrast between different thicknesses of graphene oxide. The foil to the edge appears to be approximately one layer thick while it gets progressively thicker with more layers being added. Hence TEM image confirms the presence very thin graphene oxide layers in the sample.

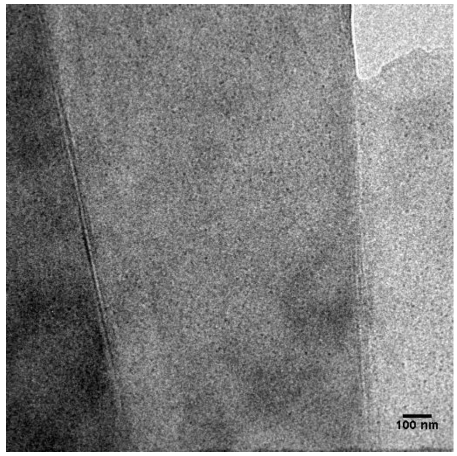

Fig 3.3(xvii): Higher Magnification image of graphene oxide foil

The density measurements of the samples were tried but could not be used to measure the volume fraction of graphene. The mass of the composite samples was very small and did not give reasonable measurements. The volume fractions in the table given above also did not show a marked variation. Therefore, the difference in density due to the change in volume fraction of graphene would also be insignificant.

Chapter 4

DISCUSSION

The presence of graphene oxide in the amorphous portion of the X-ray spectrum can be explained by the structure of graphene oxide. Electron energy loss spectroscopy combined with STEM-ADF imaging and AFM-depth profiling shows that graphene oxide films have substantially different density-of-states and resonance electron plasma excitation energy than those in graphene[(27)]. It also indicates that oxygen atoms attach to graphene sites randomly and convert sp^2 carbon bonds in graphene to sp^3 bonds. While the structural modifications of graphene are dependent on the oxidation level, the results show that a 1:5 oxygen to carbon ratio is sufficient to transform the measured 40% of carbon bonds into sp^3 bonds. As a consequence, the atomic structure of oxidized graphene is highly distorted becoming a semi amorphous solid carbon oxide.

The absence of graphite related peaks in the X-ray diffraction is thought to arise from the very thin layers of graphene that did not contribute to the diffracted beam. Also, the presence of indium could lead to absorption of the diffracted beam from graphene. Thus, the only observed peaks after subtracting those from the mounting clay arose from indium

The SEM and optical images gave different values for the volume fraction. However both these results are prone to error. The determination of volume fraction from the images is not highly reliable since the distribution is not uniform in the small area observed and hence any image would be the representation of only a very small fraction of the sample. Thicker platelets of graphene are also included in these observations which do not possess the exceptional properties of graphene. Also, the interaction volume of the sample with the electron beam is large enough to show contrast from graphene particulates underneath the surface. Therefore, volume fractions were determined using resistance measurements. Resistivity is much more sensitive to volume fraction of graphene in the sample. These would give a much more accurate value of volume fraction of graphene in the sample. The resistivity of graphene is also evaluated using models for electrical resistance of composites. Specifically, the rule of mixtures and effective mean field analysis are used to model the electrical resistivity of the composite samples.

4.1 Rule of Mixtures (RM)

Graphene is dispersed in either the indium or the indium-gallium alloy matrix in the composite samples. In or In-Ga foil will be referred to as the matrix in the composite. The graphene particulates are assumed to be in series connection electrically with the matrix in the composite for resistance modeling.

The resistance and thermal coefficient resistance of the composite and matrix were measured experimentally and are listed in Table 3.1(ii).

The resistance R of the composite when graphene and matrix are in series is given by

$$R_c = R_m + R_g \tag{1}$$

In the above equation, subscript m refers to the matrix, g to the graphene particulates and c to the composite.

Expressing it in terms of the resistivity $\rho,$ length l and area of cross-section a.

$$\rho_c(\frac{l_c}{a_c}) = \rho_m(\frac{l_m}{a_m}) + \rho_g(\frac{l_g}{a_g}) \tag{2}$$

The graphene particulates are spread throughout the matrix. Hence assuming they cover the same cross section as does the matrix,

$$a_c = a_m = a_g = a \tag{3}$$

Hence, the resistivity of the composite becomes

$$\rho_c = \rho_m(\frac{l_m}{l_c}) + \rho_g(\frac{l_g}{l_c}) \tag{4}$$

Multiplying and dividing by area,

$$\rho_c = \rho_m V_m + \rho_g V_g \tag{5}$$

In the above equation, V represents the volume fraction of each component. This relation however holds only when there is a uniform distribution of graphene in series with the matrix. The distribution of graphene particulates is random and the assumption that the area of cross sections of matrix and graphene is equal does not hold. Hence this model would not give an accurate representation of the volume fraction.

Differentiating (1) with respect to temperature and dividing by R_c

$$\left(\frac{1}{R_c}\right)\frac{dR_c}{dT} = \frac{\left(\frac{1}{R_c}\right)dR_m}{dT} + \frac{\left(\frac{1}{R_c}\right)dR_g}{dT} \tag{6}$$

The left hand side term of the equation now gives the thermal coefficient of resistance of the composite (TCR_c). Expressing the matrix and graphene terms in terms of their thermal coefficients of resistance,

$$\frac{1}{R_c}\frac{dR_c}{dT} = \frac{R_m}{R_c}(\frac{1}{R_m}\frac{dR_m}{dT}) + \frac{R_g}{R_c}(\frac{1}{R_g}\frac{dR_g}{dT}) \tag{7}$$

Eqn. (7) can be written as

$$\mathrm{TCR_c} = \frac{\mathrm{R_m}}{\mathrm{R_c}}\mathrm{TCR_m} + \frac{\mathrm{R_g}}{\mathrm{R_c}}\mathrm{TCR_g} \tag{8}$$

$$\frac{R_m}{R_c} = \rho_m\left(\frac{l_m}{l_c}\right) \tag{9}$$

Eqn. (9) can be expressed in the form of volume fractions since the areas of cross section were assumed to be linear.

$$\frac{R_m}{R_c} = \frac{\rho_m}{\rho_c}\ V_m \tag{10}$$

Similarly,

$$\frac{R_g}{R_c} = \frac{\rho_g}{\rho_c} V_g \tag{11}$$

Using (10) and (11) in Eqn. (9),

$$TCR_c = \frac{\rho_m}{\rho_c} V_m \, TCR_m + \frac{\rho_g}{\rho_c} V_g \; TCR_g \tag{12}$$

Dividing Eqn. (5) by ρ_c

$$1 = \frac{\rho_m}{\rho_c} V_m + \frac{\rho_g}{\rho_c} V_g \tag{13}$$

Using (13) in Eqn. (12),

$$TCR_c = TCR_m + \frac{\rho_g}{\rho_c} V_g \; (TCR_g - TCR_m) \tag{14}$$

$$\rho_g V_g = \rho_c \frac{TCR_c - TCR_m}{TCR_g - TCR_m} \tag{15}$$

Substituting the values obtained for $\rho_g V_g$ in Eqn. (5) and the known value of resistivity of metal matrix, the volume fraction of matrix and that of graphene is calculated. The thermal coefficient of resistance of indium is 4.35×10^{-3} K^{-1} while its resistivity is 9.42×10^{-6} Ω cm and that of indium-gallium is 4.32×10^{-3} K^{-1} and 9.42×10^{-6} Ω cm respectively from Table 3.1(ii). The TCR of graphene is assumed to be similar to that of graphite which is around -0.0003 or -0.0005[28]. These values were substituted in Eqn. (6) to determine the resistivity and volume fraction of graphene for both the values of TCR.

The values are given in Table 4.1(i) for the two values of TCR of graphene. The values of resistivity of graphene calculated from different samples are found to be different. Hence, the rule of mixtures does not give an accurate representation of the resistivity of the composite. The composite consisting of graphene platelets of different sizes and orientation cannot be modeled correctly using rule of mixtures. A more realistic model is the Effective Mean Field Analysis.

Table 4.1(i): Volume fraction and resistivity of graphene

	TCR= -0.0003		TCR = -0.0005	
Sample	V_g	ρ_g (10^{-6} Ω cm)	V_g	$\rho_{g(}10^{-6}$ Ω cm)
In-Gr-1	0.26	1.39	0.26	1.34
In-Gr-2	0.08	2.03	0.08	1.96
In-Gr-3	0.15	4.29	0.15	4.19
In-Ga-Gr-1	0.13	1.81	0.13	1.74
In-Ga-Gr-2	0.17	2.01	0.17	1.94
In-Ga-Gr-3	0.14	0.88	0.14	0.84
In-Ga-Gr-4	0.15	2.41	0.14	2.33
In-Ga-Gr-5	0.10	1.74	0.10	1.68

4.2 Effective Mean Field Analysis (EMA)

The orientation of the graphene platelets could not be determined either by x-ray diffraction or from the scanning electron microscopy. The size of graphene platelets was seen to range from submicron to a few micrometers. When the platelets are larger, deformation by rolling is expected to give rise to preferred orientation, with graphene platelets parallel to the surface of the foil. However the smaller platelets might be too small to be effected by rolling.
The conductivity σ_c of a two phase system[25,29] made up of randomly oriented ellipsoidal anisotropic grains is the solution of the equation,

$$\frac{\varphi}{3}\sum_{i=1}^{3}\frac{\sigma_1^i-\sigma_c}{\sigma_c+L_1^i(\sigma_1^i-\sigma_c)}+\frac{1-\varphi}{3}\sum_{i=1}^{3}\frac{\sigma_2^i-\sigma_c}{\sigma_c+L_1^i(\sigma_2^i-\sigma_c)}=0 \tag{16}$$

where the subscripts refer to phase 1 and phase 2 and φ refers to the volume fraction of phase 1. The anisotropic conductivities of the grains are expressed by the diagonal elements (i=1,2 and 3) of their conductivity tensor σ_j^i,where j refers to the different phases present. The shapes of the grains are taken into account via their depolarization factors, $\mathrm{L_j^i}$ with $\sum_{i=1}^{3} \mathrm{L_j^i} = 1$.

The above equation becomes

$$\frac{\mathrm{V_m}}{3}\sum_{\mathrm{i}=1}^{3}\frac{\sigma_m^i-\sigma_c}{\sigma_c+L_m^i(\sigma_m^i-\sigma_c)}+\frac{V_g}{3}\sum_{\mathrm{i}=1}^{3}\frac{\sigma_g^i-\sigma_c}{\sigma_c+L_g^i(\sigma_g^i-\sigma_c)}=0 \qquad (17)$$

for the indium-graphene composite. The matrix grains are assumed to be isotropic and hence $\sigma_m^1 = \sigma_m^2 = \sigma_m^3 = \sigma_m$ and spherical and hence $\mathrm{L_m^i}$= 1/3 for all values of i. Graphene in the form of thin platelets or flat ellipsoids is anisotropic, so that $\mathrm{L_g^i} = 0$ for i=1, 2 and $\mathrm{L_g^i} = 1$ for i=3. $\sigma_g^1 = \sigma_g^2 = \sigma_g^a$ and $\sigma_g^3 = \sigma_g^c$ for graphene since superscripts "1" and "2" refer to directions along the basal plane which is represented by "a" and 3 is the direction perpendicular to the basal plane which is represented by "c". Symmetry in the basal plane makes the conductivities along the directions 1 and 2 the same. Eqn. (17) then becomes

$$3V_m\frac{(\sigma_m-\sigma_c)}{(\sigma_m+2\sigma_c)}+\frac{V_g}{3}\left(\frac{2\sigma_g^a}{\sigma_c}-\frac{\sigma_c}{\sigma_g^c}\right)-\frac{V_g}{3}=0 \qquad (18)$$

The ratio $\frac{\sigma_g^a}{\sigma_g^c}$ is assumed to be constant "f". σ_g^c is expressed in terms of σ_g^a and f and V_m in terms of V_g. Differentiating Eqn. (18) with respect to temperature gives an additional equation, relating the temperature coefficients of conductivities of matrix, composite and graphene.

Noting that $\sigma = \frac{1}{\rho}, \frac{1}{\rho}\frac{d\rho}{dT} = \frac{1}{\sigma}\frac{d\sigma}{dT}$ and

$$\rho = \frac{Ra}{l} \qquad (19)$$

Differentiating with respect to temperature and dividing by ρ,

$$\frac{1}{\rho}\frac{d\rho}{dT} = \frac{1}{R}\frac{dR}{dT} + \frac{1}{a}\frac{da}{dT} - \frac{1}{l}\frac{dl}{dT} \tag{20}$$

If t and w are the width and thickness

$$\frac{1}{\rho}\frac{d\rho}{dT} = \frac{1}{R}\frac{dR}{dT} + \frac{1}{t}\frac{dt}{dT} + \frac{1}{w}\frac{dw}{dT} - \frac{1}{l}\frac{dl}{dT} \tag{21}$$

$\frac{1}{l}\frac{dl}{dT}$ gives the linear coefficient of thermal expansion, α. Assuming it is the same for all three dimensions, Eqn. (21) yields,

$$\frac{1}{\rho}\frac{d\rho}{dT} = \frac{1}{R}\frac{dR}{dT} + \alpha \tag{22}$$

The values of linear coefficient of In and In-Ga alloy were taken as the value of In because of the low atomic percentage of Ga.

Table 4.2 (i): Values of constants used

Sample	α	TCR	Resistivity
In	32.1×10^{-6}	0.004345	9.42×10^{-6}
Graphene	6.5×10^{-6}	-0.0005	
Composite	9.23×10^{-6}	0.004112	7.35×10^{-6}

The higher value of modulus of graphene (0.5 TPa) and lower value of α of graphene are also responsible for the low value of α_c of the graphene composite(31). Although α_c is a function of volume fraction of graphene, the result does not significantly change from the value given above due to the very high modulus of graphene. Turner's formula(32) and the expression derived by Schapery(33) are used for the evaluation of α_c of the composite.

The value of f was found to be close to 40 from previous experimental determination of conductivity of graphene ribbons in the “a” and “c” directions [26]. Eqn. (18) and its derivative with respect to temperature are satisfied to the same numerical accuracy by an iterative procedure for each of the composite samples by substituting the known values of conductivities and the values of TCR.

The volume fraction and resistivity of graphene based on this evaluation are shown in the Table 4.2(ii).

Table 4.2(ii): Values of resistivity and volume fraction of graphene using EMA analysis

Sample	V_g	$\rho_g(10^{-6}\ \Omega$ cm)
In-Gr-1	.13	1.19
In-Gr-2	.11	1.73
In-Gr-3	.14	1.68
In-Ga-Gr-1	.12	1.76
In-Ga-Gr-2	.13	1.65
In-Ga-Gr-3	.13	1.68
In-Ga-Gr-4	.13	1.76
In-Ga-Gr-5	.12	1.87

Comparison between the values of volume fraction and resisitivity of graphene obtained using RM and EMA analysis is shown in Table 4.2(iii) below. It is seen that that the resistivity of graphene obtained using RM is different for each composite, whereas those obtained using EMA are closer to each other for the three samples of the composite with In or for the five samples of the composite with In-Ga alloy. These results from EMA illustrate that the matrix conductivity does not have a significant effect on the conductivity of graphene.

Table 4.2(iii): Values of resistivity and volume fraction of graphene using RM and EMA analysis

	TCR= -0.0003		TCR = -0.0005			
Sample	V_g	ρ_g ($10^{-6}\Omega$ cm)	V_g	ρ_g($10^{-6}\Omega$cm)	V_g (EMA)	ρ_g($10^{-6}\,\Omega$ cm) (EMA)
In-Gr-1	0.26	1.39	0.26	1.34	.13	1.19
In-Gr-2	0.08	2.03	0.08	1.96	.11	1.73
In-Gr-3	0.15	4.29	0.15	4.19	.14	1.68
In-Ga-Gr-1	0.13	1.81	0.13	1.74	.12	1.76
In-Ga-Gr-2	0.17	2.01	0.17	1.94	.13	1.65
In-Ga-Gr-3	0.14	0.88	0.14	0.84	.13	1.68
In-Ga-Gr-4	0.15	2.41	0.14	2.33	.13	1.76
In-Ga-Gr-5	0.10	1.74	0.10	1.68	.12	1.87

Table 4.2(iv): Value of $\rho_g V_g$ for RM and EMA analysis

Sample	$\rho_g V_g$($10^{-6}\,\Omega$ cm)	$\rho_g V_g$ ($10^{-6}\,\Omega$ cm)
In-Gr-1	0.34	.16
In-Gr-2	0.15	.19
In-Gr-3	0.06	.24
In-Ga-Gr-1	0.23	.21
In-Ga-Gr-2	0.33	.21
In-Ga-Gr-3	0.12	.22
In-Ga-Gr-4	0.33	.23
In-Ga-Gr-5	0.17	.22

The product $\rho_g V_g$ determines the contribution of graphene in the overall electrical resistivity of the composite. The values of this product obtained using RM and EMA analysis are presented above in Table 4.2(iii). It is found that the value of $\rho_g V_g$ changed significantly in the RM analysis but remained closer in the EMA for the group of In-Gr and In-Ga-Gr samples. The graphene platelets in the composite are seen to be isolated and surrounded by the matrix or disconnected. Therefore, the carrier path through the matrix is a controlling parameter. We assume that the interfacial resistance for carrier movement between graphene and the matrix is not a very significant factor.

The volume fractions of the graphene determined from optical and SEM images do not agree closely with the values determined from the analysis using RM and EMA. The conductivity of graphene particle above five to ten atomic layers thickness is considerably low, as it represents graphite and does not contribute to the improvement in the conductivity of the sample. When the thickness of graphene is below ten atomic layers, the optical and SEM images do not provide strong enough contrast. Therefore, a fraction of the graphene particles that are observed in the images with strong contrast are expected to be thicker and do not contribute to lowering the resistivity of the composite.

The discrepancy between the observed volume of graphene and that determined from the electrical conductivity and TCR of the composite samples is due to the deficiency of the imaging methods in distinguishing graphene particles with smaller thickness. EMA analysis of electrical resistivity provides a more accurate determination of the volume fraction of graphene because the conductivity of the composite is greatly increased by the thinner graphene particulates.

The results illustrate that the resistivity of exfoliated graphene particulates in the composites is much smaller than that of pure In or In-Ga alloy. Therefore, the exfoliated graphene significantly contributes to the electrical conductivity of the composites.

Chapter 5

CONCLUSIONS

Composite samples of graphene with In and In-Ga alloy matrix were prepared by combining exfoliated graphene oxide particulates with metal foil. The composite foils were prepared by repeated rolling and annealing in argon. Indium oxide or gallium oxide formed by reduction of graphene oxide was fluxed using indium flux upon heating to slightly above the melting point of the alloy. The resulting foils were characterized by x-ray diffraction, optical microscopy, SEM and TEM. Electrical resistivity and TCR of the samples were measured. Modeling of the electrical conductivity was carried out using RM and EMA. The following conclusions were reached:

1. Composites of graphene with metals can be easily prepared by dispersing exfoliated graphene oxide on the metal foils, with repeated folding and rolling. Heating the foils at higher temperature converts the graphene oxide to graphene. Metal oxide formed by reduction of graphene oxide can be fluxed and etched away from the surface.

2. Optical or scanning electron microscopy does not provide a quantitative method of evaluating the volume fraction of graphene platelets with thickness less than ten atomic layers, as the strong contrast comes mainly from thicker platelets. Secondary-electron contrast in SEM also arises from graphene from the subsurface layers when the beam interacts with finite volume.

3. Electrical resistivity and temperature coefficient of electrical resistance of the composite were used to determine the volume fraction and electrical resistivity of graphene quantitatively. RM and EMA were used for modeling. It was found that EMA gives more consistent results for conductivity of graphene.

Electrical conductivity of graphene in the composite does not strongly depend on the matrix. The electrical conductivity of graphene is an order of magnitude higher than that of indium or the indium-gallium alloy. The electrical conductivity of the composites is increased significantly by the addition of graphene.

Chapter 6

FUTURE SCOPE

Thermal conductivity measurements have to be conducted to validate the increase in thermal conductivity of the composite due to presence of graphene. The volume fraction can also be verified from the modeling results. Experimental procedure has to be modified to reduce the amount of thick graphene platelets and increase size of the exfoliated graphene.

REFERENCES

1. http://en.wikipedia.org/wiki/Graphite.

2. Geim, A. K, *Science* **324**, 1530-1534(2009).

3. Aiping Yu, Palanisamy Ramesh, Mikhail Itkis, E, Elena Bekyarova and Robert Haddon, C, *The Journal of Physical Chemistry Letters C*, **111**, 7565-7569, 2007.

4. William Hummers, S, JR. and Richard Offman, E, *J. Am. Chem. Soc.*, **80(6)**, 1339, 1958.

5. Stankovich, S, Dikin, D.A, Dommett, G.H.B, Kohlhass, K.M, Zimney, E.J, Stach, E.A, Piner, R.D, Nguyen, S.T and Ruoff, R.S, *Nature* **442**, 282 (2006).

6. Venugopal, A, Colombo, L and Vogel, E.M, *Applied Physics Letters* **96**, 013512 (2010).

7. Nosolev, K.S, Geim, A.K, Morozov, S.V, Jiang, D, Katsnelson, M.I, Grigorieva, I.M, Dubonos, S.V and Firsov, A.A, *Nature* 438, 197 (2005).

8. Geim, A.K and Novoselov, K.S, *Nature* 6, 183-191(2007).

9. Akturk, A and Goldsman, N, *J. Appl. Phys.* **103**, 053702 (2008).

10. http://www.lbl.gov/Science-Articles/Archive/ALS-graphene.html

11. http://ww2.chemistry.gatech.edu/~orlando/epicslab/graphene.html.

12. Meyer, J, Geim, A.K, Katsnelson, M.I, Novoselov, K.S, Booth, T.J and Roth,S, *Nature* **446**,60 (2007).

13. Meyer, J.C, Kisielowski, C, Erni, R, Rossell, M.D, Crommie, M.F and Zettl, A, *Nano Lett*. **8**, 3582 (2008).

14. Balandin A.A, Ghosh S, Bao, W, Calizo, I, Teweldebrahm, D, Miao, F and Lau, C.N, *Nano Lett*. **8**, 902 (2008).

15. Saito, K, Nakamura, J and Natori, A, *Phys. Rev.* **76B**, 115409 (2007).

16. Lee, C, Wei, X, Kysar, J.W and Home, J, *Science* **321**, 385 (2008).

17. Frank, I.W, Tanenbaum, D.M, Van Der Zande, A.M and McEUen, P.L, J. *Vac. Sci. Technol.* **25 B**, 2558 (2007).

18. Eda, G, Fanchini, G and Chhowalla, M, *Nat. Nanotechnol*. **3**, 270 (2008).

19. Yazyev, O.V and Katsnelson, M.I, *Phys. Rev. Lett*. **100**, 047209 (2008).

20. Dan, Y, Lu, Y, Kybert, N.J, Lou, Z and Johnson, A.T.C, *Nano Lett*. **9**, 1472 (2009).
Kovacik, J and Bielel, J, *Scr. Mater.* **35**, 151 (1996).

21. Schedin, F, Geim, A.K, Morozov, S.V, Hill, E.W, Blake, P, Katsnelson, M.I and Novoselov, K.S, *Nat. Mater*. **6**, 652 (2007).

22. Adam, S, Hwang, E.H, Galistski, V.M and Das Sharma, S, Proc. *Natl. Acad. Sci.* **104**, 18392 (2007).

23. Giovanetti, G, Khomyakov, P.A, Brocks, G, Karpan, V.M, van den Brink, J and Kelly, P.J, *Physics Review Letters* **101**, 026802 (2008).

24. Qiushi Ran, Mingzhi Gao, Yan Wang, and Zhiping Yu, *Applied Physics Letters* 94, 103511 (2009).

25. Sasha Stankovich, Dmitriy DIkin, D, Richard Piner, D , Kevin Kolhaas, A, Alfred Kleinhammes, Yuanyuan Jia, Yue Wu, SonBinh Nguyen, T and Rodney Ruoff, S, Carbon **45**, 1558(2007).

26. Celzard, A, Mareche, J and Furdin, G, *Prog. Mater. Sci*. **50**, 93 (2005).

27. Tajima, K , Hino, Y, Narushima, T and Iguchi, Y, *Mater. Trans. JIM* **41**, 714 (2000).

28. Andre Mkhoyan, K, Alexander Contryman, W,John Silcox, Derek Stewart, A, Goki Eda,Cecilia Mattevi, Steve Miller and Manish Chhowalla, *Nano Lett.*, DOI: 10.1021/ nl8034256.

29. Tipler, P.A and Mosca, G, *Physics for Scientists and Engineers*, 5^{th} ed., Vol. 2 (New York:Freeman, 2004), p.792.

30. Helsing, J and Helte, A, *J. Appl. Phys.* **69**, 3583 (1991).

31. Nelson, J.B and Riley, D.P, *Proc. Phys. Soc*. **57**, 477 (1945).

32. Turner P.S, *J. Res. Natl. Bur. Stand.* **37**, 239 (1946).

33. Schapery, R.A, *J. Compos. Mater.* **2**, 311 (1969).